

Ultra-Low Damage High-Throughput Sputter Deposition on Graphene

Ching-Tzu Chen^{1*}, Emanuele A. Casu^{1,2}, Martin Gajek¹ and Simone Raoux¹

¹ IBM Thomas J. Watson Research Center, Yorktown Heights, New York 10598, USA

² Politecnico di Torino, Turin 10129, Italy

Abstract:

This study systematically investigated the sputtering induced graphene disorder. We identified the energetic sputtering gas neutrals as the primary cause of defects, and we introduced the grazing-angle sputtering that strongly suppressed fast neutral bombardment to retain the structural integrity of the underlying graphene, creating considerably lower damage than electron-beam evaporation while preserving the high deposition rate. Such sputtering technique yielded continuous, smooth thin films, demonstrating its potential for metal contact, gate oxide, and tunnel barrier fabrication in graphene device applications.

KEYWORDS: Graphene; sputtering; defect; thin films

Graphene exhibits novel physical properties that intrigue scientists and technologists alike.¹ The exceptional intrinsic mobility, high rigidity, fast photo-response, small spin-orbital coupling and minute nuclear spin fluctuations make graphene a promising material to host future-generation nano-devices in electronics,² nanoelectromechanical systems (NEMS),³ optoelectronics,⁴ and spintronics.⁵ To fabricate practical devices, a reliable high-throughput method for depositing a wide range of metallic and dielectric thin films on graphene is crucial. Nowadays modern semiconductor industry relies mainly on sputter deposition in large-scale production of integrated circuits, memory, and other devices.⁶ Sputtering can achieve high deposition rate regardless of the melting point of the target materials. In addition, sputtering generally preserves film stoichiometry when processing complex compound materials⁷ such as ferroelectrics, oxides, and magnetic multilayers, significantly expanding the applicability of the technology across various industries. Despite numerous advantages, the application of sputter deposition on graphene has been hitherto limited. Researchers mostly rely on electron-beam (e-beam) evaporation for metal contact formation, and atomic layer deposition (ALD) or e-beam evaporation for dielectrics deposition, putting considerable constraints on graphene device materials. The reason for the scarcity lies in the extensive damage sustained by the underlying graphene in conventional sputtering methods.^{8,9} Previous reports^{8,9} show that Raman spectra of graphene after sputtering generally exhibit substantial spectral weight in the defect mediated D-peak, with the exception of Ref. 10. Often the graphene G and 2D peaks also lose their characteristic peak shape, indicative of amorphization of sp^2 C–C bonds.¹¹ In this paper, we systematically investigate the leading cause of structural damages and show that by placing of the substrates in the *grazing-angle* sample-target configuration with

proper sputtering parameters, one can significantly reduce the damages in graphene while maintaining satisfactory deposition rates, promoting sputter deposition as a viable technology in graphene device fabrication.

For this study, we used flake graphene exfoliated from Kish graphite and deposited on Si substrates capped with thermal oxide layers. Structural damages in various sputtering configurations were characterized by Raman spectroscopy using a commercial micro-Raman system under 532 nm green-light laser illuminations. Spectral weights of various graphene Raman modes were obtained by fitting to Lorentzian functions. Since symmetry dictates that Raman D mode appears only when there exists structural defects, the spectral weight ratio (I_D/I_G) thus provides a quantitative measure of sputtering damage. From the I_D/I_G ratio, one can then derive the average domain size (L_a) of the resulting graphene nanocrystallites using the following formula, $L_a \text{ (nm)} = (2.4 \times 10^{-10}) \lambda_{\text{laser}}^4 \text{ (nm)} (I_D/I_G)^{-1}$.¹²

In this work, thin films on graphene were deposited in two magnetron sputtering systems. The majority of the parameter-tuning experiments were done in a custom-made sputtering chamber with small magnetron guns using 1" diameter targets for flexibility purposes. Effects of the substrate-target configurations, incidence angle of the deposited species, discharge power, discharge current, sputtering gas species, gas pressure, deposition rate, and deposition time were all analyzed. The optimal condition derived from the studies was then implemented in a high-throughput commercial sputtering system with larger sputter guns using 2" diameter targets for best-quality films. Both systems routinely achieved base pressure of 10^{-7} Torr or below. Unless otherwise stated, most of the samples discussed in this paper were grown under DC sputtering mode in 2 – 4 mTorr of Ar with the substrate-to-target distance maintained at 20 – 23 cm.

The most important result of this paper is the dramatic reduction of damage in graphene by the introduction of grazing-angle sputter deposition. We focus on two distinct substrate-target alignment configurations: *normal incidence* vs. *tangential-incidence*. In conventional normal-incidence sputtering, the substrate faces the target directly such that the sputtered species arrive at the substrate along its normal direction for fast deposition. On the other hand, in tangential-incidence sputtering, the tangent of the substrate surface lies in the substrate-target direction (see schematics in Fig. 1(a)), which ensures that all high-energy particles arrive at the graphene surface in the tangential direction to minimize the impact of knock-on collisions.

Figure 1(a) compares the typical Raman spectra of single-layer graphene before and after these two types of sputter deposition of Ti. The deposition conditions and film thicknesses are given in the figure caption. We note that *the deposition rate in the tangential-incidence configuration drops merely ~15% compared to normal incidence*. The small decrease in rate is consistent with deposition in the diffusive regime, where the sputtered target species undergo numerous scattering events with a mean free path on the order of ~2 cm at ~4 mTorr.¹³ From the much broadened and diminished G and 2D peaks of the graphene sample under normal-incidence sputtering (lower curve in Fig. 1(a)), we see that the graphene lattice have been severely disrupted, manifesting the onset of second-stage amorphization¹¹ by the high energy species created during the sputtering process. The Raman I_D/I_G ratio (~384%) suggests that the average graphene domain size L_a of the resulting film is only ~5.0 nm. In contrast, keeping pressure, discharge power, and substrate-to-target distance constant, deposition under the grazing-angle configuration dramatically suppresses the impact to the underlying graphene and preserves the graphene

characteristic Raman G and 2D peaks (see upper curve in Fig. 1(a)). The I_D/I_G ratio ($\sim 74\%$) derived from this sample indicates that the domain size of the underlying graphene has been improved to $L_a \sim 26$ nm. Fine-tuning the magnetron configuration and sputtering parameters can further reduce sputtering damage. As illustrated in Fig. 1(b), it is possible to suppress the defect-induced Raman D-mode to $I_D/I_G \leq 5\%$ ($L_a \geq 385$ nm), visibly below the degree of disorder caused by the few keV X-ray radiation emitted during e-beam evaporation¹⁴ ($I_D/I_G \sim 14\%$, $L_a \sim 137$ nm) under similar deposition rates and deposition time.

Below we describe the experiments that identify the origin of structural damage in graphene. The main energy influxes impinging on the graphene samples during the sputtering process include the following: high-energy ions and electrons, high-energy neutrals (from both the sputtered target species and the sputtering gas), and radiation. In non-reactive DC magnetron sputtering on unbiased substrates, it is found that energetic *neutral* particles dominate the bombardment of substrates.¹⁵ This is because, unlike RF sputtering,¹⁶ ions and secondary electrons of the sputtering gas and sputtered target species are strongly confined to the cathode region (target) by the electrostatic potential and magnetic field, and thus high-energy charged particles seldom reach the substrate.

During the sputtering process, two types of energetic neutrals are created. One is the sputtered target species, the kinetic energy of which generally lies below 10 eV.⁷ The other is the fast neutrals of the sputtering gas, depending on the cathode discharge voltages, the energy of which may be as high as a few hundred eV.¹⁷ We first examine the possibility of sputtered species causing damage in graphene by varying the pressure of the sputtering gas (Ar) and recording the corresponding changes in the Raman I_D/I_G ratio. If

the sputtered target species is indeed the culprit, increasing Ar pressure would strongly thermalize the sputtered particles¹⁸ and significantly reduce the incoming particle energy, which in turn would lower I_D/I_G in graphene. However, the comparison experiments presented in Fig. 2 reveal the exact opposite trend.. Compared with the graphene flakes under 3 mTorr deposition of Ti with similar film thickness and the same discharge power density ($\sim 2.95 \text{ W/cm}^2$ on the target), the I_D/I_G ratio of the resulting single-layer graphene flakes can be 60% larger during the 10 mTorr deposition of Ti, which shows that graphene damage is much more severe during the high-pressure deposition, thereby empirically ruling out sputtered target species as the main damage force.

The other possibility is the high-energy neutral gas species. During sputtering, fast Ar neutrals are formed either by recombination of fast Ar^+ ions with the secondary electrons near the negatively charged target^{17,19} or by collisions of neutral Ar atoms with the accelerating Ar^+ .¹³ Because they are charge neutral, these energetic species can rebound off the target with a large kinetic energy up to the discharge voltage, liberated from the electrostatic confinement of the target. Since high-energy fast neutrals have a much smaller scattering cross-section and a longer mean free path ($\sim 35 \text{ cm}$ at 4 mTorr),^{20,17,18} they undergo substantially fewer collision events with the plasma and preserve the quasi-ballistic nature during the deposition process, in sharp contrast to the strongly thermalized sputtered target species.¹⁸ As a result, the ratio of the incoming fast neutrals to the sputter-deposited film atoms increases with pressure.¹⁷ The higher the Ar pressure, the more severe is the fast-neutral bombardment rate relative to the film deposition rate on graphene, consistent with what we find in Fig. 2.

We also investigated the collision impact imparted by a heavier gas species, Kr. Keeping the discharge current, gas pressure, and deposition time constant, we observed a larger damage sustained by graphene in Ti/Kr sputtering than that in Ti/Ar sputtering (see Table 1). Contrary to the prediction of binary collisions,²¹ using heavier sputtering gas appears to provide little advantage when the target species is light. It is also interesting to note that if we consider only binary collision mechanism as many prior studies have assumed,²⁰⁻²² the reflection coefficients of heavy sputtering-gas species bouncing off light target elements (such as Ar and Kr bombardment of Al or Ti) should be exceedingly small, especially with Kr gas. Our observation of noticeable sputtering damages in graphene, which is particularly severe under normal incidence (Fig. 1(a)), indicates that non-binary multiple-collision events play an important role in the reflection of energetic gas neutrals, consistent with the direct particle-flux measurements reported in Ref. 17 and Ref. 19.

Next we examine the impact of electron bombardment on graphene. Previous magnetron sputtering experiments have found that escaping primary and secondary electrons may account for a significant fraction of the energy influx towards the substrate.²³ However, to cause damages such as vacancies²⁴ or bond rotations²⁵ in graphene during the knock-on collisions, these electrons must transfer sufficient energy to the C atoms to overcome their displacement threshold E_d .^{26,27} Both density-functional molecular dynamics simulation (DFT-MD) and the tight-binding (DFTB) model calculate E_d to be 22-23 eV in graphene.²⁸ One can then estimate how energetic the incident electrons needs to be using the elastic Coulomb scattering model. In this approximation, the maximum energy transfer to the C atoms, T_{max} , is related to the incident electron energy E_e by $T_{max} =$

$\frac{2M_C E_e (E_e + 2m_e c^2)}{(M_C + m_e)^2 c^2 + 2M_C E_e}$, where M_C is the mass of C atom and m_e is the electron mass.²⁸ To transfer $T_{max} \sim E_d \sim 23$ eV to C atoms for ejection from graphene, it requires ~ 113 keV of incident electron energy. (We note that because of the large mass mismatch between electrons and C atoms, the energy transfer by collisions is rather inefficient.) In comparison, the energy of the irradiated secondary electrons in sputtering usually lies below 100 eV²⁹ and that of the escaping primary electrons below the discharging energy ~ 500 eV. Both are orders of magnitude lower than the energy value necessary for vacancy generation.^{24,25,27} Even if the increase of energy transfer due to lattice vibrations²⁴ is taken into account and the lower-transformation-energy bond-rotational Stone-Wales defect^{25,30} is considered, the reduced onset energy for emission, $80 - 100$ keV,^{24,25} is still beyond the energy scale of the irradiated electrons in any sputtering system. Therefore, electron bombardment during sputter deposition cannot disrupt the graphene structural integrity.

Regarding the impact of radiation from the sputtering plasma, since photons are massless and transfer negligible kinetic energy, plasma radiation can create damages only if they induce chemical reactions or generate local heating above the thermal stability threshold in graphene. For photochemical reactions to take place, photon energy has to reach ~ 12.5 eV so that σ -bond electrons can be promoted to π^* -bond.³¹ In comparison, the UV photons emitted by Ar plasma and Kr plasma are only $11.6 - 11.8$ eV and $10 - 10.6$ eV respectively.³² Therefore, plasma radiation emitted during sputtering isn't energetic enough to break the C-C sp^2 bonds. Furthermore, graphene optical absorbance between 8 eV to 12 eV is minute,³¹ and consequently, radiation induced bond-breaking and heating should be negligible especially in the case of on-substrate graphene samples. We can thereby rule out plasma radiation as a damage source.

Earlier, we have demonstrated empirically that among the two types of energetic neutral particles produced during the sputtering process, it is mainly the sputtering gas species that does the damage to graphene. Here we review the theoretical results in literature to understand why. We consult the molecular dynamics calculations of Ar ion irradiation for reference because charge doesn't make a difference in collision processes where nuclear interaction dominates. According to theoretical atomistic simulations,³³ the incoming neutral species starts to knock C atoms out of graphene when its energy rises above tens of eV, which is precisely the energy range of the sputtering gas species under acceleration by the high discharge voltages. In contrast, the energy of the sputtered neutrals from the target remains well below the displacement threshold, ranging from a few eV up to ~20 eV regardless of the discharge potential.⁷ Collisions with the background Ar gas at a few mTorr further bring it down to below 5 eV.¹⁸ As a result, the energy of the sputtered film species is generally too weak to disturb the underlying graphene lattice.

Based on the energetics arguments detailed above and the pressure-dependence trend shown in Fig. 2, we therefore conclude that among the various energetic species impinging upon the sample, it is primarily the fast Ar neutrals that give rise to the damage in graphene. To reduce sputtering induced defects, we note that the graphene displacement energy threshold is anisotropic. As predicted by DFTB calculations, the energy threshold for ejection of C atoms along the in-plane direction is much higher (E_d ranges from 43 eV to $\gg 100$ eV) than that along the normal direction ($E_d \sim 23$ eV).^{28,33} Hence, by placing the graphene substrate in the tangential grazing-incidence configuration, we can strongly suppress the sputtering induced structural damage, as shown in Fig. 1.

We also note that there is a positive correlation between the degree of damage and the deposition time. Under the same sputtering condition using Kr gas at 4 mTorr, extending the deposition time by 50% enhances the damage ratio by $\sim 47\%$ (Table 2). Since these two deposited films have complete coverage of the substrates, the increase in damage implies that the impact of the energetic neutrals can cascade through the coated films to disrupt the underlying graphene. In Fig. 3, we compile the dependence of I_D/I_G ratio on the product of deposition time and discharge power density for various thin films deposited under tangential incidence in the custom-made magnetron sputtering system with 1" diameter targets (labeled by open black diamonds) and in the commercial magnetron system with 2" diameter targets (labeled by red crosses). This figure demonstrates that regardless of material types, the degree of graphene damage measured by I_D/I_G is roughly proportional to the power-density-time product. The longer the deposition time, the more graphene is exposed to high-energy gas neutrals; the higher the discharge power, the higher is the incident energy of these neutral particles. Therefore, given a fixed film thickness and target material, one should balance the discharge power density, discharge voltage, and gas pressure, such that the exposure to high-energy gas neutrals relative to the deposited film atoms is minimized. As shown in the inset of Fig. 3, moving from the small magnetron guns holding 1" targets to the larger magnetron gun system capable of sputtering at lower pressure ($P \leq 2$ mTorr) with much higher rates (≥ 1 nm/min) at a given discharge power density greatly suppresses the exposure to high energy Ar neutrals, yielding films of minimal damage in graphene. A larger magnetron gun also ensures a better balanced magnetic field distribution, thereby yielding better confinement of primary electrons, reducing the drift of sputtering gas ions towards the substrate, decreasing the

minimum gas pressure that a sputtering gun can be operated, and therefore decreasing the sputtering induced graphene damage.

To fabricate thin dielectric layers as tunnel barrier or gate oxide on graphene, achieving film uniformity is as crucial as minimizing damage. In the case of ALD of Al_2O_3 ³⁴ and molecular beam epitaxy (MBE) deposition of MgO ³⁵, dressing the graphene surface with a seed layer is necessary to ensure uniform coverage. Using tangential grazing-angle sputtering, we compared the film morphology of in-situ oxidized 1 nm Al on graphene with and without 1 monolayer (ML) of Ti buffer layer. Scanning electron microscopy (SEM) and atomic force micrographs (AFM) revealed frequent cracks in pure AlO_x on graphene (Figs. 4(a) and 4(b)) and indicated that film coverage can be compromised locally. Film coverage did not seem to improve with the Ti seed layer, but the r.m.s. roughness of locally flat regions ($\sim 1 \mu\text{m}^2$) was reduced from $\sim 3.18 \pm 0.30 \text{ \AA}$ to $\sim 2.76 \pm 0.15 \text{ \AA}$. Interestingly, film coverage was dramatically improved in elevated-temperature ($T = 200 \text{ }^\circ\text{C}$) sputter deposition of Ti/Al and Al on graphene followed by a gradual cool-down. In both cases, we observed homogeneous, fully-covered films with minute graphene damage ($I_D/I_G \leq 5\%$). While deposition and oxidation of the 1nm Al thin film at $T = 200 \text{ }^\circ\text{C}$ with a Ti seed layer gave rise to a rougher film with r.m.s. roughness $\sim 3.90 \pm 0.45 \text{ \AA}$ (Fig. 4(c)), deposition and oxidation of 1nm Al at $T = 200 \text{ }^\circ\text{C}$ without Ti yielded an improved r.m.s. roughness $\sim 2.46 \pm 0.15 \text{ \AA}$ (Fig. 4(d)), about half the lattice constant of aluminum ($a = 4.05 \text{ \AA}$) and aluminum oxide ($a = 4.785 \text{ \AA}$). The results above demonstrate the strong potential of high-temperature grazing-angle sputtering in developing uniform gate dielectrics, tunnel barriers, and multilayer thin films for graphene device applications.

Recently, flipping-configuration sputtering on graphene was reported to mimic the mild impact of thermal evaporation and eliminate graphene disorder.¹⁰ By facing the substrate 180° away from the target during sputtering at high pressure ($P = 20$ mTorr), this process was shown to create negligible damage during Al and CoFe deposition. However, due to the substrate-target geometry and severe scattering, its deposition rate dropped more than an order of magnitude to 2.5 nm *per hour* for Al, a relatively high-yield metal. This is in comparison to the 60 nm – 100 nm *per hour* rate in our tangential-incidence configuration. Such low deposition rate renders flipping sputtering undesirable for industrial production. In contrast, our grazing-angle sputtering method can easily be scaled up by adopting large-diameter sputter guns and substrate rotations for large-area high-throughput deposition. Lastly, the nucleation and film growth mode in grazing-angle sputtering better resembles the energetics of conventional sputtering. Therefore, we expect it to produce better quality magnetic multilayers than other strongly thermalized deposition methods.

Acknowledgement:

The authors would like to thank S. M. Rossnagel, Jani Kotakoski, Hsin-Ying Chiu, Li Yang, K. F. Mak, P. Avouris, and V. Perebeinos for illuminating discussions. We are grateful for the technical support of S. L. Brown, J. R. Rozen, T. Ruiz, and B. A. Ek on modifying the high-vacuum sputtering system and for the assistance of S.-J. Han with e-beam evaporation. E. A. Casu acknowledges the fellowship support of his internship at IBM from the Politecnico di Torino.

References:

1. A. K. Geim, Science 324, 1530–1534 (2009).
2. Y.-M. Lin et al., Science 332, 1294–1297 (2011).
3. J. S. Bunch et al., Science 315, 490–493 (2007).
4. F. Bonaccorso, Z. Sun, T. Hasan and A. C. Ferrari, Nature Photonics 4, 611–622 (2010). F. Xia et al., Nature Nanotechnology 4, 839–843 (2009).
5. N. Tombros et al., Nature 448, 571–574 (2007).
6. S. M. Rossnagel, IBM J. Res. Develop. 43, 163–179 (1999).
7. K. Wasa, M. Kitabatake, and H. Adachi, Thin Film Materials Technology - Sputtering of Compound Materials (2004).
8. Z. Jin et al., Appl. Phys. Lett. 95, 233110 (2009).
9. B. Dlubak et al., Appl. Phys. Lett. **97**, 092502 (2010).
10. X. P. Qiu et al., AIP Advances **2**, 032121 (2012);
11. A. C. Ferrari and J. Robertson, Phys. Rev. B 61, 14095 (2000).
12. L. G. Cançado et al., Appl. Phys. Lett. 88, 163106 (2006).
13. B. Chapman, Glow Discharge Processes, John Wiley & Sons (1980).
14. X. Llovet et al., J. Appl. Phys. 93, 3844–3851 (2003).
15. H. Kersten, H. Deutsch, H. Steffen, G. M. W. Kroesen, R. Hippler, Vacuum 63, 385–431 (2001).
16. J. M. Anderssen, E. Wallin, E. P. Munger, and U. Helmersson, J. Appl. Phys. 100, 033305 (2006).
17. S. M. Rossnagel, J. Vac. Sci. Technol. A 7, 1025–1029 (1989).
18. R. E. Somekh, J. Vac. Sci. Technol. A 2, 1285–1291 (1987).

19. I. Brodie et al., Phys. Rev. Lett. 21, 1224–1226 (1968), and references therein.
20. R. S. Robinson, J. Vac. Sci. Technol. 16, 185 (1979).
21. W. Eckstein and J. P. Biersack, Z. Phys. B 63, 471–478 (1986).
22. T. P. Drusedau et al., J. Vac. Sci. Technol. A 17, 2896–2905 (1999).
23. S. D. Ekpe and S. K. Dew, J. Vac. Sci. Technol. A 20, 1877–1885 (2002).
24. J. C. Meyer et al., Phys. Rev. Lett. 108, 196102 (2012).
25. J. C. Mayer et al., Nano Lett. 8, 3582 (2008). J. Kotakoski et al. Phys. Rev. Lett. 106, 105505 (2011).
26. The displacement threshold E_d is defined as the minimum energy that the C atoms have to acquire in order to escape from their initial lattice positions. Generally, E_d is appreciably higher than the formation energy of single vacancies (~ 7.5 eV),²⁷ which is the equilibrium energy difference between the defect state and the pristine graphene state, as there exists a kinetic barrier that the system has to cross over to initiate the transition.
27. F. Banhart, J. Kotakoski, and A. V. Krashenninnikov, ACS Nano 5, 26-41 (2011), and references therein.
28. J. Kotakoski et al., Phys. Rev. B 82, 113404 (2010); A. V. Krashenninnikov et al., Phys. Rev. B 72, 125428 (2005); A. Zobelli et al., Phys. Rev. B 75, 245402 (2007).
29. S. M. Rossnagel and H. R. Kaufman, J. Vac. Sci. Technol. A 4, 1822–1825 (1986).
30. J. Kotakoski et al., Phys. Rev. B 83, 245420 (2011).
31. Li Yang, Phys. Rev. B 83, 085405 (2011).

32. C. Cismaru and J. L. Shohet, *Appl. Phys. Lett.* 74, 2599–2601 (1999).
33. O. Lehtinen et al., *Phys. Rev. B* 81, 153401 (2010). O. Lehtinene et al., *Nanotechnology* 22, 175306 (2011).
34. D. B. Farmer and R. G. Gordon, *Nano Lett.* 6, 699–703 (2006); Y.-M. Lin et al., *Nano Lett.* 9, 422–426 (2009).
35. W. H. Wang et al., *Appl. Phys. Lett.* 93, 183107 (2008).

List of Tables:**Table 1.** Comparison of sputtering induced graphene damage by Ar and Kr

Gas Species	Ar	Kr
Target Species	Ti	Ti
Gas Pressure (mTorr)	4	4
Discharge Current (mA)	40	40
Deposition Time (min)	30	30
Film Thickness (nm)	5	3.7
I_D/I_G	$95\% \pm 4\%$	$133\% \pm 23\%$

Table 2. Dependence of sputtering induced graphene damage with deposition time

Gas Species	Kr	Kr
Target Species	Ti	Ti
Gas Pressure (mTorr)	4	4
Discharge Current (mA)	40	40
Deposition Time (min)	30	45
Film Thickness (nm)	3.7	5.5
I_D/I_G	$133\% \pm 23\%$	$196\% \pm 50\%$

List of figures:

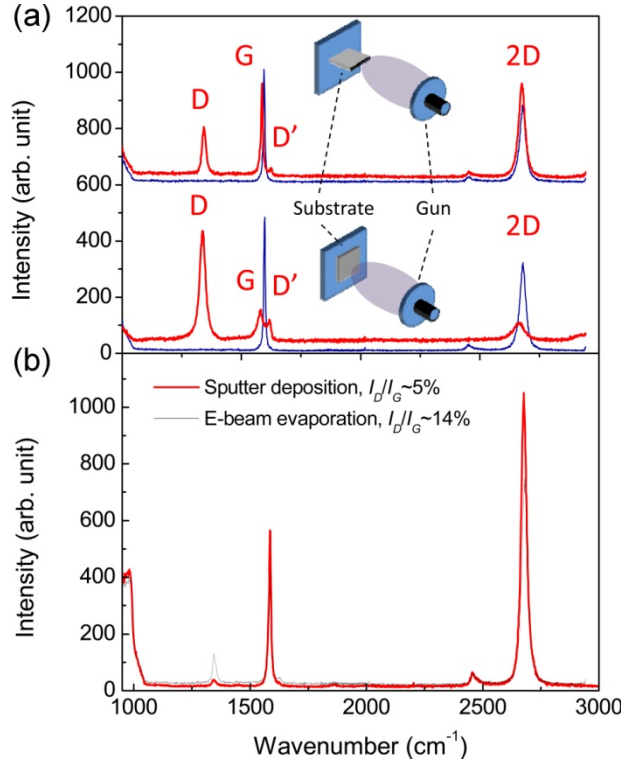


Figure 1 (a) Raman spectra of a single-layer graphene sample before (blue dotted lines) and after (red solid lines) normal- and tangential-incidence sputter deposition of Ti in Ar at 4 mTorr with a discharge power density of $\sim 5.12 \text{ W/cm}^2$ on the target. The tangential-incidence data have been shifted up by 600 units for clarity. The film deposition rate is $\sim 0.2 \text{ nm/min}$ under normal incidence and $\sim 0.17 \text{ nm/min}$ under tangential incidence, and the film thickness is $\sim 5 \text{ nm}$ and $\sim 3.6 \text{ nm}$ under tangential and normal incidence respectively. Inset: Schematics of substrate-target alignment in normal and tangential-incidence configurations. (b) Comparison of Raman spectra of single-layer graphene after tangential-incidence sputter deposition of 1 nm Al and e-beam evaporation of 1 nm Al. Sputtering has been done in Ar at 2 mTorr and $\sim 2.47 \text{ W/cm}^2$ discharge power density, with a deposition rate of $\sim 1 \text{ nm/min}$. E-beam evaporation deposition rate is comparable, $\sim 0.6\text{--}1.2 \text{ nm/min}$.

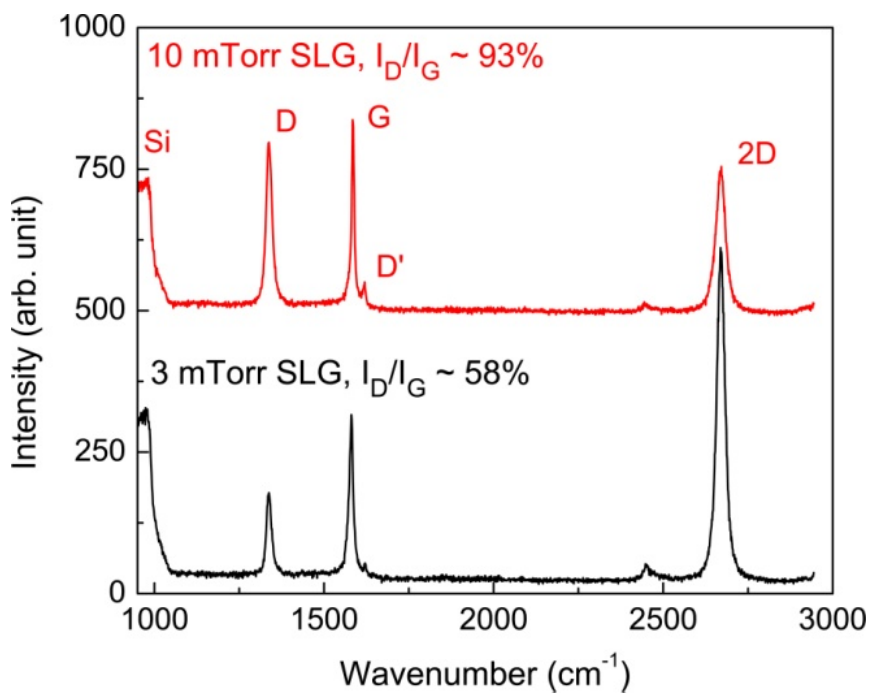


Figure 2. Raman spectra of single-layer graphene (SLG) after tangential-incidence sputter deposition of Ti in Ar at 3 mTorr (black) and 10 mTorr (red, shifted up by 500 units for clarity). Both are deposited under the discharge power density of $\sim 2.95 \text{ W/cm}^2$ on the target. The thickness of the films is 3 nm – 3.3 nm.

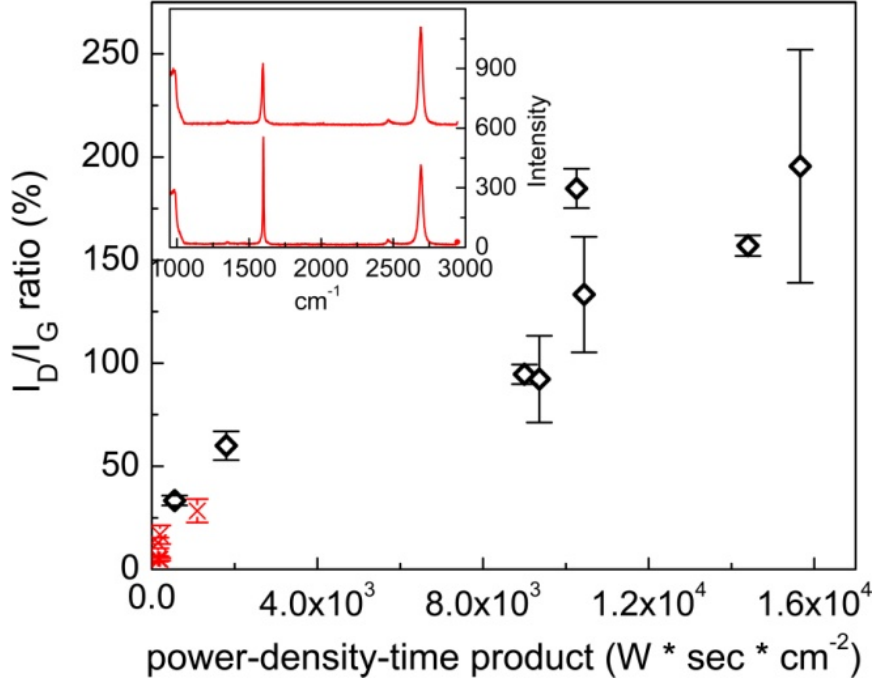


Figure 3. Dependence of I_D/I_G ratio with discharge-power-density deposition-time product. Data containing various Ti, Co, and Ti/MgO thin films grown on graphene under the tangential grazing-angle deposition configuration in the custom-made magnetron sputtering chamber are labeled in open black diamonds. Data of films grown in the commercial magnetron sputtering system are shown in red crosses. The sample-target distance is fixed at ~ 23 cm, and film thickness is kept below 5 nm. Inset: Raman spectra of sputter-deposited, in-situ oxidized 1 nm Al thin films on graphene grown at 200 °C with (upper curve) and without (lower curve) the Ti adhesion layer, demonstrating nearly perfect graphene structure after sputtering. The film morphology of these two samples is shown in the AFM images in Fig. 4(c) and Fig. 4(d).

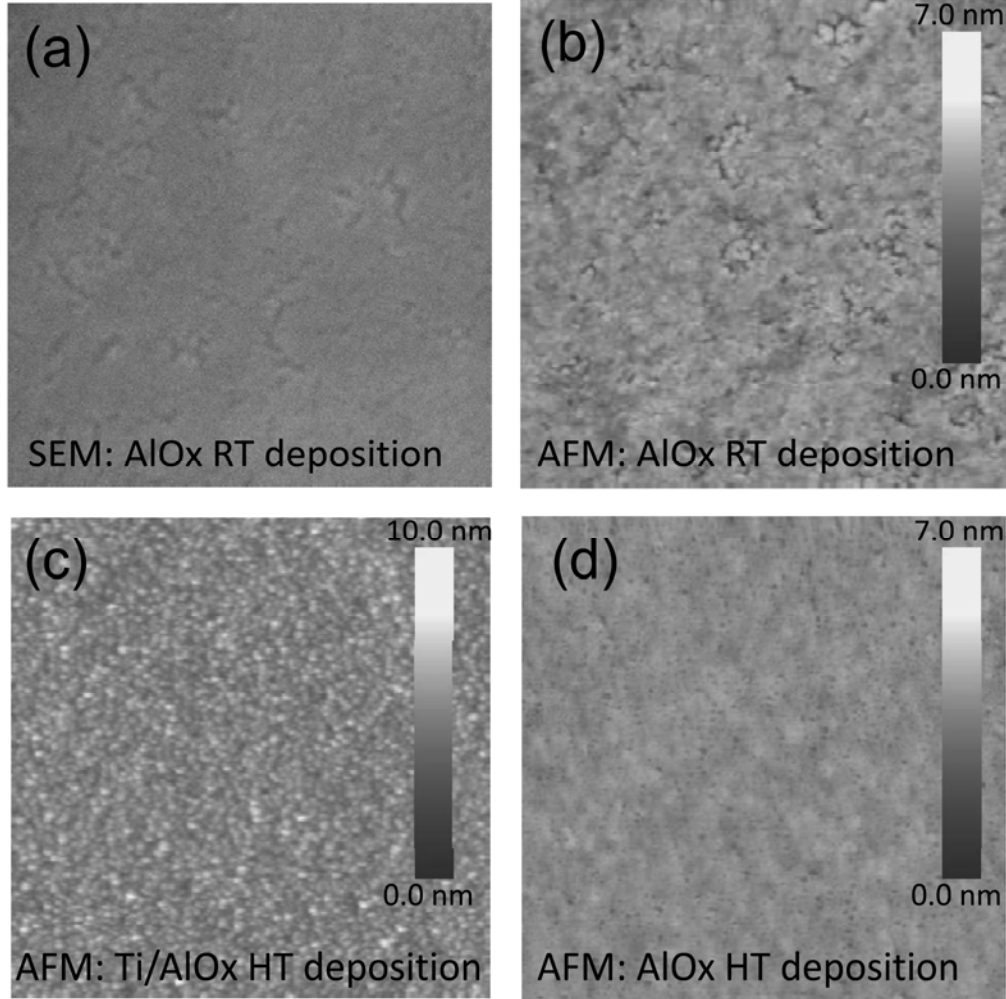


Figure 4. Morphology of sputtered AlO_x thin films on graphene deposited under tangential grazing incidence. **(a)** SEM image ($1\ \mu\text{m} \times 1\ \mu\text{m}$) of the in-situ oxidized 1nm Al film on graphene deposited at room-temperature (RT). **(b)** AFM micrograph ($1\ \mu\text{m} \times 1\ \mu\text{m}$) of the in-situ oxidized 1nm Al film on graphene deposited at RT. **(c)** AFM micrograph ($1\ \mu\text{m} \times 1\ \mu\text{m}$) of the in-situ oxidized 1 nm Al film on graphene deposited at $200\ ^\circ\text{C}$, with 1ML of in-situ oxidized Ti buffer layer. **(d)** AFM micrograph ($1\ \mu\text{m} \times 1\ \mu\text{m}$) of in-situ oxidized 1nm Al film on graphene deposited at $200\ ^\circ\text{C}$.